Development and Validation of a MRI-Based Radiomics Prognostic Classifier in Patients with Primary Glioblastoma Multiforme

Xin Chen, MD[1], Mengjie Fang, MPhil[1], Di Dong, MPhil, Lingling Liu, MPhil, Xiangdong Xu, MPhil, Xinhua Wei, MD, Xinqing Jiang, MD, PhD, Lei Qin, MPhil, PhD, Zaiyi Liu, MD, PhD

Abbreviations

GBM glioblastoma multiforme

post-T1WI postcontrast T1-weighted imaging

OS overall survival

KPS Karnofsky performance status

ROC receiver operating characteristic curve

MRI magnetic resonance imaging

ROI regions of interest

DWI diffusion weighted imaging

ICC interclass correlation coefficient

mRMR the minimum redundancy maximum relevance

MI mutual information

AIC Akaike's information criterion

AUC the area under curve

Rationale and Objectives: Glioblastoma multiforme (GBM) is the most common and deadly type of primary malignant tumor of the central nervous system. Accurate risk stratification is vital for a more personalized approach in GBM management. The purpose of this study is to develop and validate a MRI-based prognostic quantitative radiomics classifier in patients with newly diagnosed GBM and to evaluate whether the classifier allows stratification with improved accuracy over the clinical and qualitative imaging features risk models.

Methods: Clinical and MR imaging data of 127 GBM patients were obtained from the Cancer Genome Atlas and the Cancer Imaging Archive. Regions of interest corresponding to high signal intensity portions of tumor were drawn on postcontrast T1-weighted imaging (post-T1WI) on the 127 patients (allocated in a 2:1 ratio into a training [n = 85] or validation [n = 42] set), then 3824 radiomics features per patient were extracted. The dimension of these radiomics features were reduced using the minimum redundancy maximum relevance algorithm, then Cox proportional hazard regression model was used to build a radiomics classifier for predicting overall survival (OS). The value of the radiomics classifier beyond clinical (gender, age, Karnofsky performance status, radiation therapy, chemotherapy, and type of resection) and VASARI features for OS was assessed with multivariate Cox proportional hazards model. Time-dependent receiver operating characteristic curve analysis was used to assess the predictive accuracy.

Results: A classifier using four post-T1WI-MRI radiomics features built on the training dataset could successfully separate GBM patients into low- or high-risk group with a significantly different OS in training (HR, 6.307 [95% CI, 3.475-11.446]; $p < 0.001$) and validation set (HR, 3.646 [95% CI, 1.709−7.779]; $p < 0.001$). The area under receiver operating characteristic curve of radiomics classifier (training, 0.799; validation, 0.815 for 12-month) was higher compared to that of the clinical risk model (Karnofsky performance status, radiation therapy; training, 0.749; validation, 0.670 for 12-month), and none of the qualitative imaging features was associated with OS. The predictive accuracy was further improved when combined the radiomics classifier with clinical data (training, 0.819; validation: 0.851 for 12-month).

Conclusion: A classifier using radiomics features allows preoperative prediction of survival and risk stratification of patients with GBM, and it shows improved performance compared to that of clinical and qualitative imaging features models.

Key Words: Glioblastoma multiform; Survival analyses; Magnetic resonance imaging; Radiomics.

Acad Radiol 2019; 26:1292−1300

From the Department of Radiology, Guangdong Provincial People's Hospital, Guangdong Academy of Medical Sciences, Guangzhou 510080, China (X.C., Z.L.); Department of Radiology, Guangzhou First People's Hospital, School of Medicine, South China University of Technology, Guangzhou, China (X.C., L.L., X.X., X.W., X.J.); Department of Imaging, Dana-Farber Cancer Institute, Boston 02115, Massachusetts (L.Q.); Department of Radiology, Harvard Medical School, Boston 02115, Massachusetts (X.C., L.Q.); Key Laboratory of Molecular Imaging, Chinese Academy of Sciences, University of Chinese Academy of Sciences, Beijing, China. Received August 23, 2018; revised December 6, 2018; accepted December 19, 2018. Address correspondence to: Z.L.; L.Q. e-mails: lqin2@partner.org, zyliu@163.com

[1] These authors contributed equally.

https://doi.org/10.1016/j.acra.2018.12.016

GLRLM
Gray-level run-length matrix
LGLRE
Low gray-level run emphasis

INTRODUCTION

Glioblastoma multiforme (GBM) is the most frequent and deadly type of primary malignant tumor of the central nervous system. Through standard treatment consisting of maximal surgical resection followed by adjuvant chemotherapy and radiation therapy, the median survival time of patients with GBM was significantly improved from 15.3 months to 21.7 months; however, the survival time varies widely from 3 months to 12 years following diagnosis (1,2). Thus, there is a need for accurate risk stratification toward a more personalized approach in GBM management.

Recently, studies have identified many markers for GBM (3–5), of which, genomic and proteomic characterization improved the clinical assessment of GBM, such as the description of distinct molecular gene expression profiles, underlying genomic abnormalities, and epigenetic modifications (6). The implementation of these markers, however, has been limited in routine clinical practice because biopsies are invasive and are not able to characterize the heterogeneity of the entire tumor (7). On the contrary, medical imaging can noninvasively capture the entire tumor characteristics, providing complementary information to the traditional tissue biopsy (8). Currently, imaging is routinely used through the treatment process. Therefore, it does not involve extra cost to access this valuable information.

Magnetic resonance imaging (MRI) plays an important role in neuro-oncology for the diagnosis and assessment of treatment response (5,9–11). Previous studies have built models to predict overall survival (OS) using feature combinations which include preoperative tumor volume, Karnofsky performance status (KPS), involvement of eloquent brain regions, volume of the nonenhanced tumor, extent of edema, degree of necrosis, and degree of contrast enhancement (5). However, most of these imaging features very much depend on radiologists' experience.

"Radiomics" is an emerging field that aims to utilize the full potential of medical imaging by extracting a large number of quantitative features, including tumor intensity, shape, and texture (12–14). A comprehensive and robust quantification of the imaging phenotypes provides complementary and clinically relevant information, which may lead to imaging biomarkers. As shown in recent studies, quantitative imaging features have prognostic value in predicting clinical outcomes or assessing treatment response in several cancer types (4,15,16). For example, Liu et al found that the performance of combined four MR sequences (T1-weighted imaging [T1WI], T2-weighted imaging, FLAIR and postcontrast T1WI [post-T1WI]) was almost equal to that of only post-T1WI for survival stratification (17). Therefore, in the present study, we extracted many radiomics features from high signal intensity portions of the tumor on post-T1WI in patients with newly diagnosed GBM before treatment. The present study aimed to develop and validate an MRI-based radiomics classifier to predict the OS in patients with newly diagnosed GBM and to evaluate whether the classifier allows stratification with improved accuracy over that of clinical and qualitative imaging features risk models.

MATERIALS AND METHODS

Patients and Clinical Data

Clinical and MRI data of GBM were obtained from the Cancer Genome Atlas and the Cancer Imaging Archive (http://cancerimagingarchive.net/), which is an imaging portal consisting of images corresponding to the Cancer Genome Atlas patients from four centers (Henry Ford Hospital, Emory University, University of California San Francisco, Maryland Anderson Cancer Center). The studies were approved by their local ethics committee and institutional review board. We retrieved a total of 127 patients' clinical information, presurgical axial post-T1W images and their OS.

The parameters for post-T1WI were as following: TE/TR, 2.1–20 ms/4.94–3285.62 ms; slice thickness, 1–5 mm; spacing between slices, 0.7–6.5 mm; matrix size, 256 × 256 or 512 × 512; and pixel spacing, 0.47–1.02 mm.

The 127 patients were semirandomly split into a training set of 85 patients and a separate validation set of 42 patients with stratification depending on survival time. Stratified sampling was selected to reduce the limitation of the small sample size and the skewed survival distribution, and to achieve an approximately equal survival distribution of subjects between the training and validation data. The split data were more representative of the population than the random sampling. Samples were sorted by survival in an ascending order. For every three samples, the first and second samples were chosen as the training set and the third sample was selected as the validation set. Models were created in the training set and validated in the validation set.

The clinicopathologic features of the two groups are shown in Table 1. OS as the clinical endpoint was defined as the time from initial diagnosis to date of cancer-related death or date of last follow-up examination.

Imaging Preprocessing

The white-stripe approach (18) was used to perform the image intensity normalization to minimize the discrepancy of intensity distributions between subjects. Then, images were cropped and/or zero-padded to achieve a 24-cm field of

view. Considering the various imaging parameters across the four centers, all images were resampled using the cubic spline interpolation. The resulted pre-processed images had a matrix of size 256 × 256 and a slice thickness of 3 mm.

Tumor Imaging Segmentation

Two neuroradiologists (Reader 1 and Reader 2 with 8 years and 21 years of experience, respectively) manually outlined the regions of interest (ROIs) of high signal intensity portions of tumors on the single image slice with the largest tumor volume using 3D slicer (National Institutes of Health, Bethesda, Maryland). The vessels were carefully avoided when we drew ROIs of the tumor (Fig 1). Reader 1 outlined the ROIs in all 127 cases, and Reader 2 outlined in 30 randomly selected cases to evaluate interobserver agreement of radiomics features.

Radiomics Features Extraction

Radiomics features were calculated using an in-house Matlab code (MATLAB 2014a MathWorks, Natick, Massachusetts). Digital Imaging and Communications in Medicine files (MR images and tumor contours) were imported into a computer to extract the radiomics features. Four types of radiomics features were calculated in our study, namely tumor intensity, shape, texture, and Wavelet features, with a total of 3824 features (Appendix A). Note that, all features were normalized by a z score method into a standardized value range.

Imaging Review

The same two neuroradiologists reviewed the MR images using in-house picture archive and communication system. The VASARI feature scoring system for human gliomas (https://wiki.cancerimagingarchive.net/display/public/VASARI+Research+Project) was employed for the interpretation of the MR images to ensure interobserver consistency. The reviewers were blind to the clinical outcome of patients. The conclusion of the final assessment was based on the agreement between the two reviewers. MRIs were assessed for availability of relevant sequences: T1WI, post-T1WI, FLAIR, and T2-weighted imaging. Thus, a total number of 104 patients' MR images were reviewed considering the fact that the other patients missed one or more sequences of required four sequences. Furthermore, although the VASARI scoring system includes 30 imaging features, we performed 26 features instead (see Supplementary Table 1) because 3/30 features are assessed based on the postoperative MRIs and 1/30 is based on diffusion weighted imaging (DWI). Prior to analysis, the neuroradiologists were trained to determinate the VASARI features following the Vasari MR Feature Guide v1.1 on 30 randomly selected patients. Before statistical analysis, some features were changed to maintain a better distribution subgroups or to achieve a binary classification (see Supplementary Table 2).

Statistical Analysis

Study Population Demographics

Clinicopathologic variables between the training and validation sets were compared using the Student's t test for continuous variables and the chi-squared (χ^2) test for categorical variables.

Interobserver Agreement of Radiomics Features Extraction

The interclass correlation coefficient (ICC) was used to estimate the reproducibility of the extraction of radiomics features from the independent segmentations of 30 patients by two radiologists. An ICC larger than 0.75 was regarded as good agreement (19).

Radiomics Features Selection and Radiomics Classifier Building

The radiomics features with ICCs larger than 0.75 were ranked by the minimum redundancy maximum relevance (mRMR) algorithm by calculating the mutual information (MI) between a set of features and an outcome variable. MRMR ranks the input features by maximizing the MI with respect to survival time and minimizing the average MI of higher ranked features. It allows an efficient selection of relevant and nonredundant features.

To remove redundant imaging features with linear correlation, only a small number of highest ranking features were reserved. In this study, the top 40 highest-ranked radiomics features were used as the input variables of the radiomics classifier building. The Cox proportional hazard regression classifier was built based on the training set. To control for model overfitting, the number of patients should usually exceed the

TABLE 1. Clinical Pathology Features Between Training and Validation Sets

Characteristic	Training Set	Validation Set	*p* Value
Gender (male/female)	53/32	29/13	0.586
Age (years, mean/SD)	57.78/13.53	60.02/13.75	0.142
KPS (≥80/<80)	67/18	34/8	0.963
Radiation (yes/no)	79/6	38/4	0.893
Chemotherapy (yes/no)	77/8	37/5	0.901
Type of resection (biopsy/Tumor resection)	7/78	5/37	0.732
OS (days, median, and IQR)	342.0(165.0,600.0)	351.5(187.2,619.0)	0.757

Note: Numbers in the columns of training and validation sets were patient numbers except for Age and OS.
IQR, interquartile range; KPS, Karnofsky performance status; OS, overall survival; SD, standard deviation.

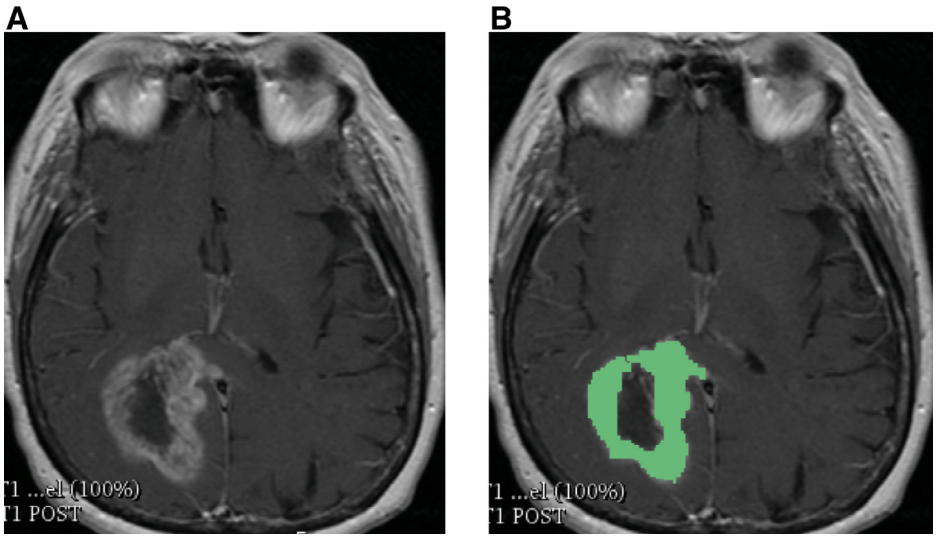

Figure 1. Glioblastoma multiform (GBM) segmentation of tumor on postcontrast T1-weighted images of a 74-year-old GBM patient with an overall survival of 110 days. Before (A) and after outlined tumor (B) image were shown for tumor segmentation. (Color version of figure is available online.)

number of the included covariates by at least 10−15 times in the multivariate analysis (20); therefore, the likelihood ratio test with Akaike's information criterion (AIC) was used as the stopping rule for a backward step-wise selection, with the lowest AIC value representing the "best approximating model" (21). Then, a risk score was computed for each patient according to the radiomics classifier.

Development and Validation of Prognostic Models

We selected the optimum cut-off score of the classifier to split the data set into high-risk and low-risk groups by using the "cutp" function of the "survMisc" R package, which define the cut-off point objectively and have been proven to have good properties in the case of survival analysis with death and censored data.

Univariate Cox proportional hazards model was used to assess the associations between survival and different individual categories of predictors including clinical variables and qualitative imaging features. Predicting variables shown as significant in the univariate Cox proportional hazards models were retained and included in the multivariate Cox proportional hazards models.

We used Kaplan-Meier method to analyze the correlation between variables and OS and the log-rank test to compare survival curves. Time-dependent receiver operating characteristic curve (ROC) analysis was used to investigate the predictive accuracy of variables, with the area under curve (AUC) calculated at different cut-off times (6, 12, and 18 months in this study, respectively). A higher AUC value indicates a better model in predicting OS.

To validate associations between survival and the models (clinical features alone, imaging features alone, radiomics classifier alone, and different combinations of the above stated models), the different models in the training set were used in the validation set and the whole set to split the survival curves.

All statistical tests were performed with R software (version 3.0.1; http://www.Rproject.org). The mRMR algorithm was implemented in the mRMRe package, and the optimum cut-off score for the radiomics classifier was performed using the "cutp" function of the "survMisc" R package. The "survival ROC" package was used to perform the time-dependent ROC curve analysis. Statistical significance with two-sided tests was set at $p < 0.05$.

RESULTS

Study Population Demographics

Patients' clinical characteristics are summarized in Table 1. There were no significant differences in clinicopathologic features between the training and validation sets (p = 0.142−0.963). Patients in the training (85 of 127, 67%) and validation sets (42 of 127, 33%) were balanced for survival (p = 0.757), with a median OS of 448 days [95% confidence interval [CI]: 355−558 days] for the training set and 448 days (95% CI: 346−638 days) for the validation set.

Interobserver Agreement of the Radiomics Features Extraction

Of the 3824 radiomics features, 1167 demonstrated good interobserver agreement, with ICCs ranging from 0.7502 to 0.9776, and the remaining 2657 with ICCs ranging from 0.1057 to 0.7499.

Radiomics Feature Selection and Prognostic Radiomics Classifier Building

We developed a classifier from the 40 top-ranked radiomics features using a Cox regression model with AIC, which selected four radiomics features in the training set. Then, a

risk score for each patient depending on their individual features values was calculated through a linear combination of selected features weighted by their respective coefficients, where risk score = (2.4611 × g.100_gab.25.2_GLCM_correlation) + (1.3805 × g.050_gab.10.2_GLCM_difference_entropy) + (2.375 × g.050_gab.15.2_GLCM_entropy) + (−2.079 × g.100_orig_GLRLM_LGLRE).

Development and Validation of Prognostic Models

Correlation Between Radiomics Classifier and Survival

The optimum cutoff of risk score was 0.140. Patients with risk scores of 0.140 or larger were classified into high-risk group, and patients with risk scores less than 0.140 were classified into low-risk group. Survival time of the high- and low-risk groups from the training and validation sets is listed in Table 2. Distributions of the risk score and survival status in the training set and validation set were shown in Figure 2 (left panel). Patients in the high-risk group had a shorter median OS than patients in the low-risk group (603 vs 199 days; hazard ratio [HR], 6.307 [95% CI: 3.475−11.446]; $p < 0.001$; Fig 2, middle panel). Similarly, patients with a high-risk score had shorter median OS than patients with a low-risk score in the validation set (256 vs 638 days; HR, 3.646 [95% CI, 1.709−7.779] $p < 0.001$) and in the whole set (221 vs 626 days; HR, 4.489 [95% CI, 2.899−6.951] $p < 0.001$).

Correlation Between Clinical Variables, Imaging Features and Survival

Univariate Cox proportional hazards model analyses demonstrated that two clinical variables of KPS and radiation therapy were significantly correlated to survival with p value < 0.050 in both training and validation sets (Table 3). Of 104 patients' 26 VASARI imaging features, none was associated with survival time except for pial invasion in validation set ($p = 0.021$ for pial invasion; Supplementary Table 2).

Multivariate Cox Analysis of the Association Between Combined Biomarker and Survival

The four-feature radiomics classifier was, along with clinical variables of KPS and radiation therapy, the parameter within a multivariate Cox regression model that consistently showed independent significance for predicting OS in both training (HR, 2.491[95% CI, 1.758, 3.528]; $p < 0.001$) and validation (HR, 2.160 [95%: 1.211−3.853]; $p = 0.009$) set (Table 4). The classifier also showed significantly higher prognostic accuracy than any individual or combined clinical variables (Fig 3). And the combined model including clinical variables and radiomics classifier is the best predictor for OS (Fig 3). When the models were used to the validation set, the same conclusion was found that the combined model with AUC of 0.851 was higher than that of 0.670 for clinical variables model and 0.815 for radiomics classifier at 12 months. Thus, the four-feature radiomics classifier can add prognostic value to clinical variables.

DISCUSSION

In this study, we used radiomics approach to analyzed post-T1W images of patients with newly diagnosed GBM. A total of 3824 radiomics features were derived from each segmented high signal lesion which can result in a high-dimensional parameter space. A series features selection methods identified a four-feature radiomics classifier in the parameter space to noninvasively predict individual risk for each subject. The radiomics classifier could successfully stratify patients into high- and low-risk groups with significant differences in OS with additive performance beyond clinical variables and standard imaging features. Integrating the radiomics classifier into model with clinical variables increased accuracy of the model.

Of the four features selected to the classifier, all features were derived from texture features, which characterize the gray-level heterogeneity of GBM. Any features related to tumor shape and size were not contained in the final classifier. The results indicate that local heterogeneity plays an important role in overall survive. Consistent with our findings, Liu et al (22) found that co-occurrence matrix and RLM-based features which reflect the regional heterogeneity contributed to prognosis differentiate between the long- and short-term groups. Furthermore, Chaddad et al (23) suggested that multitexture features can discriminate intratumoral niches with underlying tumor biology and the texture features derived from active tumor regions are the most associated with OS.

TABLE 2. Overall Survival and Mortality of Patients With High- and Low-Risk Scores in the Training, Validation, and Whole Sets

		Training Set		Validation Set		Combined Set	
		High-Risk Group	Low-Risk Group	High-Risk Group	Low-Risk Group	High-Risk Group	Low-Risk Group
No. of patients (%)		35 (41.2)	50 (58.8)	24 (57.1)	18 (42.9)	59 (46.5)	68 (53.5)
OS (days)	Median	199	603	256	638	221	626
	95% CI	146,337	486,753	164,442	546,1024	153,333	546,753
Mortality rate (%)	6 months	45.71	4.04	37.78	0.00	42.42	2.96
	12 months	73.00	20.58	72.93	5.88	73.02	16.43
	24 months	100.00	61.15	86.46	61.99	94.60	61.39

CI, confidence interval; OS, overall survival.

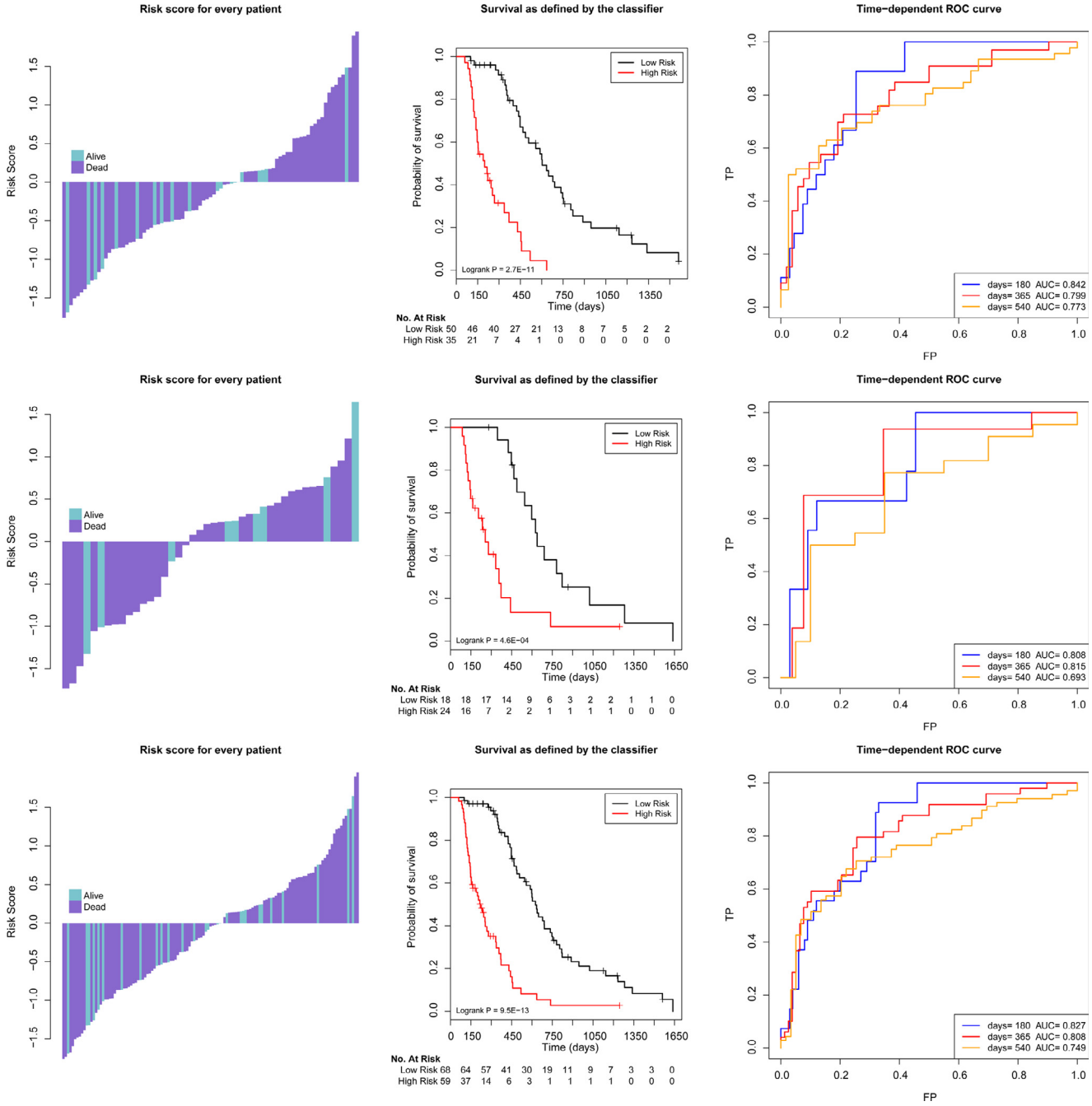

Figure 2. Risk score by the radiomics classifier (left panel), Kaplan-Meier survival (middle panel), and time-dependent receiver operation curve analysis (right panel) in the training set (first line), validation set (second line), and whole set (third line). *p* values were calculated using the log-rank test. (Color version of figure is available online.)

Previous studies have identified that radiomics features are associated to survival of patients with OS (16,24–27). Kyrre et al (28) presented support vector machine models for glioma survival association and evaluated the diagnostic accuracy of 6-month and 1-, 2-, 3-year using MR imaging-based whole tumor relative cerebral blood volume histograms. In this study, they developed four separate SVM modes of rCBV histograms with different clinically relevant survival ranges of 6 months and 1, 2, and 3 years using binary prediction which was more complicated and difficult in clinical practice. While we only developed one conventional contrast enhanced MR radiomics classifier that does not rely on arbitrary thresholds and that predicts OS as a continuous variable. In addition, Ingrisch et al (26) identified 20 features from 208 features in 66 patients with GBM which stratified the patients into high and low predicted mortality revealed a significant difference in OS. Kickingereder et al (25) built an eight-feature radiomics signature that allowed to stratify OS in both discovery and validation set. In our study, a better predictive accuracy was obtained using fewer features (four-

TABLE 3. Correlation Between Clinical Features and Survival Time on Univariate Cox Analysis in Training and Validation Sets

	Training Set				Validation Set			
Clinical Variables	Values (Counts)	Coefficient	Hazard Ratio	*p*	Values (Counts)	Coefficient	Hazard Ratio	*p*
Gender (male/female)	53/32	−0.051	0.951 (0.576−1.568)	0.842	29/13	−0.400	0.670 (0.311−1.445)	0.304
Age (≥58/<58)	42/43	0.206	1.229 (0.757−1.995)	0.404	24/18	0.631	1.880 (0.871−4.057)	0.103
KPS (≥80/<80)	67/18	−1.644	0.193 (0.094−0.399)	<0.001	34/8	−1.270	0.281 (0.113−0.695)	0.003
Radiation (yes/no)	79/6	−1.835	0.160 (0.059−0.433)	<0.001	38/4	−2.740	0.065 (0.017−0.251)	<0.001
Chemotherapy (yes/no)	77/8	0.046	1.047 (0.471−2.332)	0.910	37/5	−0.662	0.516 (0.189−1.410)	0.191
Type of resection (resection/biopsy)	78/7	0.135	1.144 (0.519−2.521)	0.738	37/5	0.343	1.409 (0.486−4.083)	0.526

KPS, Karnofsky performance status.

TABLE 4. Correlation Between Variables and Survival Time on Multivariate Cox Analysis in Training and Validation Sets

	Training Set				Validation Set			
Variables	Values (Counts)	Coefficient	Hazard Ratio	*p*	Values (Counts)	Coefficient	Hazard Ratio	*p*
KPS (≥80/<80)	67/18	−1.133	0.322 (0.149−0.698)	0.004	34/8	−0.928	0.395 (0.139−1.121)	0.081
Radiation (yes/no)	79/6	−1.680	0.186 (0.068−0.513)	0.001	38/4	−1.943	0.143 (0.035−0.589)	0.007
Radiomics signature	–	0.913	2.491(1.758−3.528)	<0.001	–	0.770	2.389 (1.782−3.203)	0.009

KPS, Karnofsky performance status.

feature radiomics classifier) for predicting OS. This is an important result because it shows that only a few features were used to evaluate prognosis for GBM patients with a less chance of over-fitting and less computation time.

Several studies have evaluated the prognostic value of the VASARI imaging features of GBM (6,29). A study by Nicolasjilwan et al of 30 VASARI imaging features, including 102 GBM patients demonstrated the proportion of tumor enhancing and a higher T1/FLAIR ratio of the tumoral signal abnormality were associated with poor outcome. In a recent retrospectively study of 189 patients with GBM by Peeken et al (29), 10 features of multilocality, satellites, ependymal invasion, deep wm invasion, definition of noncontrast enhanced tumor margin, proportion edema, max lesion size, resection contrast enhanced tumor, resection noncontrast enhanced tumor, resection edema were showed statistically significant associations for OS by univariate Cox proportional models. In our study, we found none of the VASARI imaging features were associated with OS. Those inconsistent

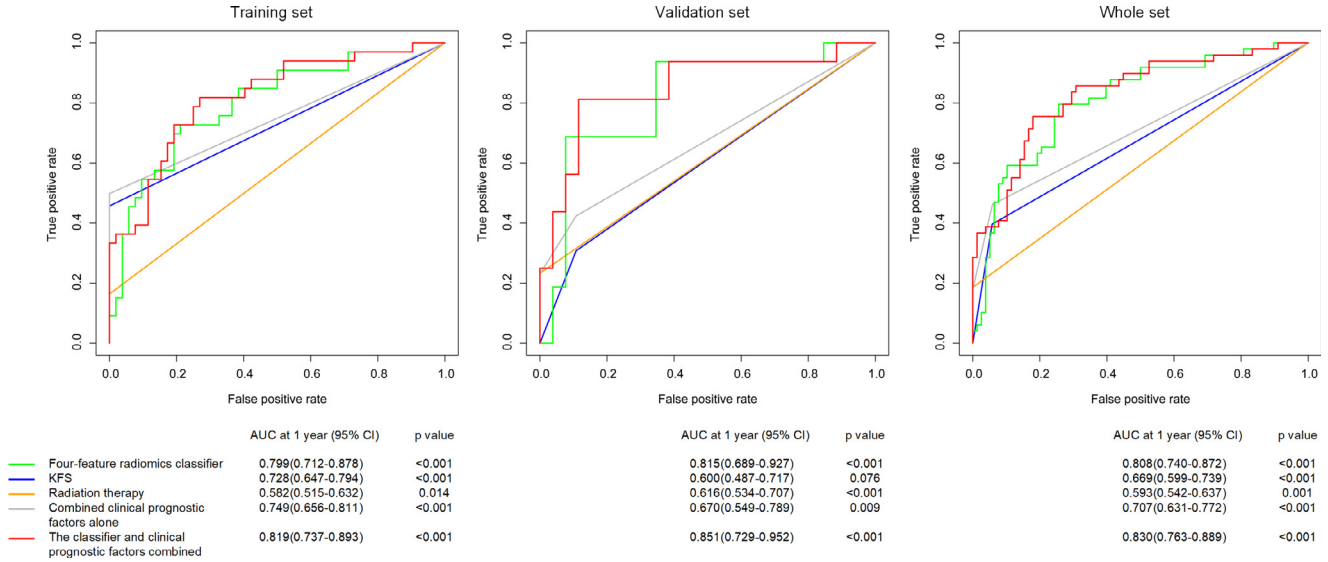

Figure 3. Time-dependent ROC curves compare the prognostic accuracy of the four-radiomics classifier with clinical risk factors in training(left), validation(middle) and whole(right) sets. AUC, area under curve; KPS, Karnofsky performance status; ROC, receiver operator characteristic. (Color version of figure is available online.)

results may ascribe to the small samples and the fact that the VASARI imaging features evaluated depend on the radiologists' experiences and may be less reproducibility.

The potential clinical relevance of our study is the advancement of the noninvasive method and the novel imaging biomarkers that have not used in clinical routine. Radiomics as a noninvasive analysis approach can extracted more comprehensive quantitative information from MRI beyond imaging signs evaluated by naked-eye and do not depend on the radiologist training experiences (12), which provides a complementary perspective. In our study, the integrative assessment of radiomics data is emphasized for predicting outcome of patients with GBM. In addition, integration of radiomics with multiscale information could yield valuable insight into tumor progression (30) and allow early identification of resistances (31). These could help a personalized approach in GBM management.

In addition to the retrospective study design, several limitations should be mentioned in our study. First, we evaluated tumor features in the largest cross-sectional area rather than performing whole-tumor analysis. Although tumor three-dimensional texture analysis may provide more diverse internal information than two-dimensional features (32), Lubner MG et al found that single slice 2D texture analysis was adequate in assessing pathologic features and clinical outcomes by using CT texture features in hepatic metastatic colorectal cancer (33). Second, Prasanna et al (16) found that peritumoral radiomics features were predictive of long-term versus short-term survival. Although we only evaluated the high signal intensity region of the tumor on post-T1WI, further studies are needed to explore whether the other parts and sequences can be used to predict the outcomes of patients with GBM. Meanwhile, Chaddad et al found that three texture features from post-T1WI were statistically significant for predicting OS, while none of any features from edema and necrosis could predict OS (34). Third, because of the retrospective nature of the study, images were acquired over the course of several years and from different institutions, and the imaging parameters slightly varied. However, we controlled this with normalizing each image to minimize the effect on our results. Finally, advanced MR such as DWI and dynamic susceptibility contrast perfusion showed the potentials in predicting OS (35,36), we will further assess the value of advanced MR for OS prediction in patients with GBM in future studies.

In conclusion, our study indicates that a four-feature radiomics classifier based on post-T1WI could predict OS and be risk stratification in patients with GBM beyond clinical variables and imaging features. In the future, this method can be integrated into other multiscale including clinical information, laboratory, etc. to improve precision medicine of GBM.

FUNDING

This work was supported by the National Key Research and Development Program of China (no. 2017YFC130910002), National Natural Scientific Foundation of China (no. 81601469, 81771912 and 81671854), Science and Technology Planning Project of Guangdong Province (no. 2014A020212341) and China Scholarship Council funding (no. 201808440033).

REFERENCE

1. Hegi ME, Diserens AC, Gorlia T, et al. MGMT gene silencing and benefit from temozolomide in glioblastoma. N Engl J Med 2005; 352:997–1003.
2. Krex D, Klink B, Hartmann C, et al. Long-term survival with glioblastoma multiforme. Brain 2007; 130:2596–2606.
3. Pope WB. Genomics of brain tumor imaging. Neuroimaging Clin N Am 2015; 25:105–119.
4. Gevaert O, Mitchell LA, Achrol AS, et al. Glioblastoma multiforme: exploratory radiogenomic analysis by using quantitative image features. Radiology 2014; 273:168–174.
5. Gutman DA, Cooper LA, Hwang SN, et al. MR imaging predictors of molecular profile and survival: multi-institutional study of the TCGA glioblastoma data set. Radiology 2013; 267:560–569.
6. Nicolasjilwan M, Hu Y, Yan C, et al. Addition of MR imaging features and genetic biomarkers strengthens glioblastoma survival prediction in TCGA patients. J Neuroradiol 2015; 42:212–221.
7. Tatli S, Gerbaudo VH, Mamede M, et al. Abdominal masses sampled at PET/CT-guided percutaneous biopsy: initial experience with registration of prior PET/CT images. Radiology 2010; 256:305–311.
8. Tykocinski ES, Grant RA, Kapoor GS, et al. Use of magnetic perfusion-weighted imaging to determine epidermal growth factor receptor variant III expression in glioblastoma. Neuro Oncol 2012; 14:613–623.
9. Akbari H, Macyszyn L, Da X, et al. Pattern analysis of dynamic susceptibility contrast-enhanced MR imaging demonstrates peritumoral tissue heterogeneity. Radiology 2014; 273:502–510.
10. Pope WB, Lai A, Mehta R, et al. Apparent diffusion coefficient histogram analysis stratifies progression-free survival in newly diagnosed bevacizumab-treated glioblastoma. AJNR Am J Neuroradiol 2011; 32:882–889.
11. Chen X, Wei X, Zhang Z, et al. Differentiation of true-progression from pseudoprogression in glioblastoma treated with radiation therapy and concomitant temozolomide by GLCM texture analysis of conventional MRI. Clin Imaging 2015; 39:775–780.
12. Lambin P, Rios-Velazquez E, Leijenaar R, et al. Radiomics: extracting more information from medical images using advanced feature analysis. Eur J Cancer 2012; 48:441–446.
13. Aerts HJ, Velazquez ER, Leijenaar RT, et al. Decoding tumour phenotype by noninvasive imaging using a quantitative radiomics approach. Nat Commun 2014; 5:4006.
14. Gillies RJ, Kinahan PE, Hricak H. Radiomics: images are more than pictures, they are data. Radiology 2016; 278:563–577.
15. Jamshidi N, Diehn M, Bredel M, et al. Illuminating radiogenomic characteristics of glioblastoma multiforme through integration of MR imaging, messenger RNA expression, and DNA copy number variation. Radiology 2014; 270:1–2.
16. Prasanna P, Patel J, Partovi S, et al. Radiomic features from the peritumoral brain parenchyma on treatment-naive multi-parametric MR imaging predict long versus short-term survival in glioblastoma multiforme: preliminary findings. Eur Radiol 2017; 27:4188–4197.
17. Liu Y, Zhang X, Feng N, et al. The effect of glioblastoma heterogeneity on survival stratification: a multimodal MR imaging texture analysis. Acta Radiologica 2018; 59:1239–1246.
18. Shinohara RT, Sweeney EM, Goldsmith J, et al. Statistical normalization techniques for magnetic resonance imaging. NeuroImage Clin 2014; 6:9–19.
19. Busing KA, Kilian AK, Schaible T, et al. Reliability and validity of MR image lung volume measurement in fetuses with congenital diaphragmatic hernia and in vitro lung models. Radiology 2008; 246:553–561.
20. Harrell FE. Regression modeling strategies: with applications to linear models, logistic and ordinal regression, and survival analysis. New York, NY: Springer-Verlag, 2015.
21. Vrieze SI. Model selection and psychological theory: a discussion of the differences between the Akaike information criterion (AIC) and the Bayesian information criterion (BIC). Psychol Methods 2012; 17:228–243.
22. Liu Y, Xu X, Yin L, et al. Relationship between glioblastoma heterogeneity and survival time: an MR imaging texture analysis. AJNR Am J Neuroradiol 2017; 38:1695–1701.

23. Chaddad A, Sabri S, Niazi T, et al. Prediction of survival with multi-scale radiomic analysis in glioblastoma patients. Med Biol Eng Comput 2018; 56:2287–2300.
24. Kickingereder P, Burth S, Wick A, et al. Radiomic profiling of glioblastoma: identifying an imaging predictor of patient survival with improved performance over established clinical and radiologic risk models. Radiology 2016; 280:880–889.
25. Kickingereder P, Neuberger U, Bonekamp D, et al. Radiomic subtyping improves disease stratification beyond key molecular, clinical, and standard imaging characteristics in patients with glioblastoma. Neuro-oncol 2018; 20:848–857.
26. Ingrisch M, Schneider MJ, Norenberg D, et al. Radiomic analysis reveals prognostic information in T1-weighted baseline magnetic resonance imaging in patients with glioblastoma. Invest Radiol 2017; 52:360–366.
27. Chaddad A, Desrosiers C, Toews M. Radiomic analysis of multi-contrast brain MRI for the prediction of survival in patients with glioblastoma multiforme. In: Conference proceedings: annual international conference of the IEEE engineering in medicine and biology society IEEE Engineering in medicine and biology society annual conference, 2016; 2016. p. 4035–4038.
28. Emblem KE, Pinho MC, Zollner FG, et al. A generic support vector machine model for preoperative glioma survival associations. Radiology 2015; 275:228–234.
29. Peeken JC, Hesse J, Haller B, et al. Semantic imaging features predict disease progression and survival in glioblastoma multiforme patients. Strahlentherapie und Onkologie 2018; 194:580–590.
30. Grossmann P, Gutman DA, Dunn Jr. WD, et al. Imaging-genomics reveals driving pathways of MRI derived volumetric tumor phenotype features in Glioblastoma. BMC Cancer 2016; 16:611.
31. Abdulla S, Saada J, Johnson G, et al. Tumour progression or pseudoprogression? A review of post-treatment radiological appearances of glioblastoma. Clin Radiol 2015; 70:1299–1312.
32. Ng F, Kozarski R, Ganeshan B, et al. Assessment of tumor heterogeneity by CT texture analysis: can the largest cross-sectional area be used as an alternative to whole tumor analysis? Eur J Radiol 2013; 82:342–348.
33. Lubner MG, Stabo N, Lubner SJ, et al. CT textural analysis of hepatic metastatic colorectal cancer: pre-treatment tumor heterogeneity correlates with pathology and clinical outcomes. Abdom Imaging 2015; 40:2331–2337.
34. Chaddad A, Tanougast C. Extracted magnetic resonance texture features discriminate between phenotypes and are associated with overall survival in glioblastoma multiforme patients. Med Biol Eng Comput 2016; 54:1707–1718.
35. Kondo M, Uchiyama Y. Apparent diffusion coefficient histogram analysis for prediction of prognosis in glioblastoma. J Neuroradiol 2018; 45:236–241.
36. Romano A, Pasquini L, Di Napoli A, et al. Prediction of survival in patients affected by glioblastoma: histogram analysis of perfusion MRI. J Neuro-oncol 2018; 139:455–460.

SUPPLEMENTARY MATERIALS

Supplementary material associated with this article can be found in the online version at doi:10.1016/j.acra.2018.12.016.